Eur. Phys. J. D **41**, 95–102 (2007)
DOI: 10.1140/epjd/e2006-00192-1

THE EUROPEAN PHYSICAL JOURNAL D

Classical dynamics of polar diatomic molecules in external fields

J.P. Salas[a]

Area de Física Aplicada, Universidad de La Rioja, 26006 Logroño, Spain

Received 26 April 2006 / Received in final form 20 June 2006
Published online 18 August 2006

Abstract. In this paper, we present the study of the global classical dynamics of a rigid diatomic molecule in the presence of combined electrostatic and nonresonant polarized laser fields. In particular, we focus on the collinear field case, which is an integrable system because the z-component P_ϕ of the angular momentum is conserved. The study involves the complete analysis of the stability of the equilibrium points, their bifurcations and the evolution of the phase flow as a function of the field strengths and P_ϕ. Finally, the influence of the bifurcations on the orientation of the quantum states is studied.

PACS. 31.15.Qg Molecular dynamics and other numerical methods – 05.45.-a Nonlinear dynamics and chaos

1 Introduction

Since the pioneering works of Langevin [1] and Debye [2] to nowadays, the manipulation of the spatial direction (rotational orientation and alignment) of a molecule by means of external fields is one of the most active subjects in physical chemistry (see, e.g., [3] to get an overall vision of the state of the art). Among other things, the control of the molecular orientation is critical for studies in chemical reaction dynamics. For polar molecules, the simplest orientation technique is provided by an static electric field (see [4] and references therein), while intense nonresonant laser fields are used to obtain molecular alignment [5]. Friedrich and Herschbach [6] and Cai et al. [8] proposed the combination of static and laser fields to enhance the molecular orientation and to gain versatility in the manipulation procedure. Recently, the predicted properties of this combined configuration have been successfully tested at the laboratory [9]. Besides the original interest on the spatial manipulation, molecules in external fields have become perfect systems to follow the tracks of the classical phase space structure in the quantum spectra [10, 11]. Furthermore, rigid molecules in external fields show in many cases the phenomenon of classical and quantum monodromy [12,13].

Following the classical point of view, in this paper we study the global dynamics of a rigid diatomic molecule subjected to combined collinear electrostatic and nonresonant polarized laser fields. In particular, we assume that the laser field is either linearly or circularly polarized. When the laser field is linearly polarized, the system undergoes a pitchfork bifurcation [6] and a saddle-node bifurcation [10,11]. While the pitchfork bifurcation has completely described as a function of the parameters controlling the dynamics, the presence of the saddle-node bifurcation has been detected by numerical experimentation for particular values of the parameters. Hence, the main objective here is to characterize it on analytical grounds as well as to get an overall vision of the dynamics. With this is mind, the paper is organized as follows. In Section 2 we describe the one-dimensional Hamiltonian we use to describe the dynamics of the rotor. This Hamiltonian depends on three parameters. Two of them are external and they represent the strength of the fields. The z-component P_ϕ of the angular momentum plays the role of an internal parameter because the axial symmetry of the problem at hand. In Section 3 we analyze the stability of the equilibrium points, their bifurcation and the phase flow evolution for $P_\phi = 0$ and for $P_\phi \neq 0$. We prove that for $P_\phi \neq 0$ the systems suffers one and only bifurcation of saddle-node type. Moreover, we obtain analytically the bifurcation curve in the parametric plane. Section 4 is devoted to the study of the influence of the saddle-node bifurcation on the orientation of the quantum states. Finally, in Section 5, the main results of the paper are summarized.

2 The classical Hamiltonian

Let us consider an ideal rigid polar diatomic molecule of moment of inertia I with a permanent dipole μ along the molecular axis and polarizability components $\alpha_\parallel$ and $\alpha_\perp$ parallel and perpendicular to the molecular axis. In the presence of an static electric field E_s along the z-axis of an inertial reference frame, the classical Hamiltonian governing the dynamics of the diatomic in spherical coordinates $(\theta, \phi, P_\theta, P_\phi)$ is given by

$$\mathcal{H} = B\left[P_\theta^2 + \frac{P_\phi^2}{\sin^2\theta}\right] - E_s\mu\cos\theta, \qquad (1)$$

where $B = \hbar^2/2I$ is the rotational constant.

[a] e-mail: josepablo.salas@dq.unirioja.es

Now, let us consider the molecule subjected to a pulsed laser field $\varepsilon(t) = h(t/\tau)\varepsilon_0 \cos(2\pi\nu t)$ linearly polarized along the z-axis, being ν the frequency of the laser and $h(t/\tau)$ the profile function of the pulse of τ duration. If we consider that ν is an infrared or microwave frequency which is nonresonant to any molecular frequency and that $v \gg 1/\tau$, the time-averaged Hamiltonian of the system is [5]

$$\mathcal{H} = B\left[P_\theta^2 + \frac{P_\phi^2}{\sin^2\theta}\right] - \frac{\langle\varepsilon(t)^2\rangle}{2}\left[\alpha_\parallel + (\alpha_\parallel - \alpha_\perp)\cos^2\theta\right], \tag{2}$$

where $\langle\varepsilon(t)^2\rangle = h^2\varepsilon_0^2/2$ is the averaged laser field.

Now, if the laser field $\varepsilon(t)$ is circularly polarized in the xy-plane,

$$\varepsilon(t) = h(t/\tau)\varepsilon_0(\cos(2\pi\nu t), \sin(2\pi\nu t), 0),$$

the corresponding averaged Hamiltonian of the molecule reads as [13]

$$\mathcal{H} = B\left[P_\theta^2 + \frac{P_\phi^2}{\sin^2\theta}\right] + \frac{\langle\varepsilon(t)^2\rangle}{2}\left[\alpha_\parallel + (\alpha_\parallel - \alpha_\perp)\cos^2\theta\right]. \tag{3}$$

Taking into account that for linear molecules $\alpha_\parallel - \alpha_\perp > 0$ and that the z-component $P_\phi = m$ of the total angular momentum is a constant of the motion, the above three configurations can be modeled by a unique dimensionless one-dimensional Hamiltonian

$$\mathcal{H} \equiv \mathcal{H}/B = P_\theta^2 + \frac{m^2}{\sin^2\theta} - w_1\cos\theta + w_2\cos^2\theta, \tag{4}$$

where energies are expressed in units of B, and where a constant energy shift has been omitted. The dimensionless parameters w_1 and w_2,

$$w_1 = \frac{E_s\mu}{B} \geq 0, \quad |w_2| = \left|\frac{\langle\varepsilon(t)^2\rangle}{2B}(\alpha_\parallel - \alpha_\perp)\right|,$$

control the strength of the fields. Note that negative values of w_2 correspond to a linearly polarized laser field. On the other side, positive values of w_2 correspond to a circularly polarized laser field.

3 Equilibrium points, stability and phase flow evolution

From (4), the Hamilton equations of motion are

$$\begin{aligned}\dot\theta &= \frac{\partial\mathcal{H}}{\partial P_\theta} = 2\ P,\\ \dot P_\theta &= -\frac{\partial\mathcal{H}}{\partial\theta} = \frac{2m^2\cos\theta}{\sin^3\theta} - w_1\sin\theta + w_2\ \sin 2\theta.\end{aligned} \tag{5}$$

The phase flow on the plane $(\theta,\ P_\theta)$ is determined for the most part by the number and stability of the equilibrium points. The equilibrium points $E_i = (\theta_i,\ P_{\theta i} = 0)$ are the roots of the system made of the right-hand side of (5) equated to zero. Equivalently, the angles θ_i are the critical points of the effective potential $V_e(\theta)$,

$$V_e(\theta) = \frac{m^2}{\sin^2\theta} - w_1\cos\theta + w_2\cos^2\theta, \tag{6}$$

that is to say the roots of the equation

$$\frac{\partial V_e}{\partial\theta} = -\frac{2m^2\cos\theta}{\sin^3\theta} + w_1\sin\theta - w_2\ \sin 2\theta = 0. \tag{7}$$

As it is well-known, the stability of a given equilibrium E_i is determined by the eigenvalues of the linear stability matrix resulting from the variational equations of motion. In our problem, these eigenvalues are

$$\lambda(\theta_i) = \pm\sqrt{-\frac{d^2V_e(\theta_i)}{d\theta^2}}. \tag{8}$$

Then, when θ_i is a minimum ($d^2V_e(\theta_i)/d\theta^2 > 0$), E_i is an stable equilibrium (center) because the corresponding eigenvalues $\lambda(\theta_i)$ are complex. When θ_i is a maximum ($d^2V_e(\theta_o)/d\theta^2 < 0$), the eigenvalues are real and the critical point E_i is an unstable equilibria (saddle point). At this point, we distinguish between the case $m = 0$ and the case $m \neq 0$.

3.1 Case m = 0

By setting $m = 0$ in equation (7), it is easy to arrive at that $V_e(\theta)$ has three critical points (i.e. three equilibria) [14], namely,

$$\theta_1 = 0, \qquad \theta_2 = \pi, \qquad \theta_3 = \cos^{-1}\left(\frac{w_1}{2w_2}\right). \tag{9}$$

Note that, while θ_1 and θ_2 always exist, θ_3 only takes place when $|w_1/2w_2| < 1$ [15]. By substituting in (8) the critical points (9), we get

$$\begin{aligned}\lambda_1 &= \pm\sqrt{2w_2 - w_1},\\ \lambda_2 &= \pm\sqrt{2w_2 + w_1},\\ \lambda_3 &= \pm\sqrt{(w_1^2 - 4w_2^2)/2w_2},\end{aligned}$$

and the following stability properties can be easily deduced:

- $E_1 = (0,0)$ is stable when λ_1 are complex, and this condition holds when $2w_2 < w_1$;
- the equilibrium E_2 is stable when $2w_2 < -w_1$;
- because E_3 exists when $w_1 < 2|w_2|$, this equilibrium is stable when $w_2 > 0$.

In Table 1 are summarized the equilibria, their conditions of existence and stability, and the corresponding energy. From the existence and stability analysis, we infer the presence of parametric bifurcations at the lines

Table 1. Conditions of existence, stability and energy of the equilibria for $m = 0$.

Equilibrium	Existence	Stable when...	Energy $\widehat{\mathcal{H}}$
$E_1 = (0, 0)$	Always	$2w_2 < w_1$	$\mathcal{H}_1 = 2w_2 - w_1$
$E_2 = (\pi, 0)$	Always	$2w_2 < -w_1$	$\mathcal{H}_2 = 2w_2 + w_1$
$E_3 = (\cos^{-1}(w_1/2w_2)\ ,\ 0)$	$w_1 < 2\|w_2\|$	$w_2 > 0$	$\mathcal{H}_3 = -w_1^2/4w_2$

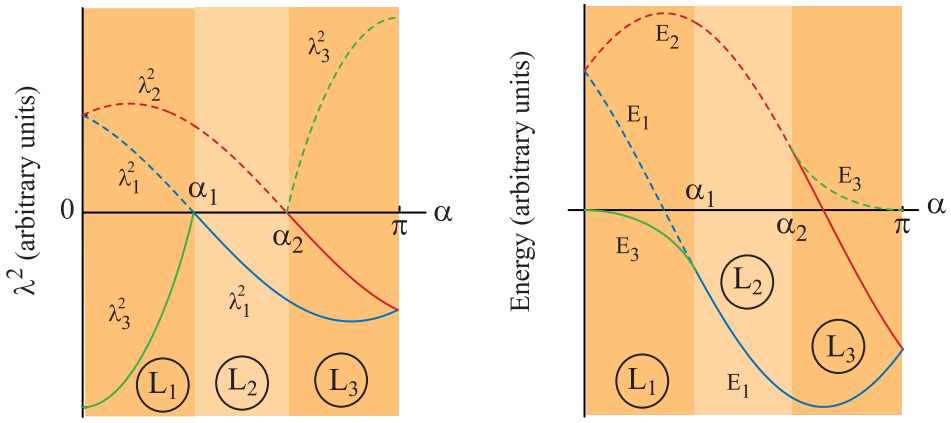

Fig. 1. (Color online) Evolution of the square of the eigenvalues λ (left panel) and the energy $\mathcal{H}$ (right panel) as a function of the rheostat parameter α (see the text for more details). The blue, red and green colors correspond, respectively, to the eigenvalues and to the energy of the equilibria E_1, E_2 and E_3. The bifurcations take place at $\tan\alpha_1 = 2$ ($w_1 = 2w_2$) and $\tan\alpha_2 = -2$ ($w_1 = -2w_2$).

$w_1/2w_2 = \pm 1$. We can confirm the presence of bifurcations by studying the evolution of the eigenvalues λ and the energy $\mathcal{H}$ of the equilibria as a function of the parameters (w_2, w_1). To do this, we introduce a rheostat parameter α in the interval $[0, \pi]$ such that

$$(w_2, w_1) = (w\cos\alpha, w\sin\alpha), \qquad 0 \leq \alpha \leq \pi.$$

From this study, which appears in Figure 1, the parametric plane (w_2, w_1) can be divided in three regions where the dynamics is different. In region $L_1 = \{(w_2, w_1) \mid w_1 < 2w_2,\ \alpha < \arctan 2\}$ (see Fig. 1) the three equilibria exist, being $E_{1,2}$ unstable while E_3 is stable. As we approach the segment $w_1 = 2w_2$ ($\tan\alpha_1 = 2$), equilibrium E_3 moves toward E_1, in such way that at $w_1 = 2w_2$, the two equilibria collide. In other words, a pitchfork bifurcation between E_3 and E_1 takes place. From this bifurcation, only the equilibrium point E_1, which becomes stable, survives and in the region $L_2 = \{(w_2, w_1) \mid 2|w_2| < w_1,\ |\tan\alpha| > 2\}$ only exist the stable equilibrium E_1 and the unstable E_2. When the line $w_1 = -2w_2$ ($\tan\alpha_2 = -2$) is crossed, by a pitchfork bifurcation, from E_2, which becomes stable, born the unstable equilibrium E_3. From this bifurcation, in region $L_3 = \{(w_2, w_1) \mid w_1 < -2w_2,\ \alpha > \arctan(-2)\}$ we have three equilibria: the unstable E_3 and the two stable $E_{1,2}$.

The presence of these bifurcations is illustrated in Figure 2, where the evolution of the phase flow is shown. For clarity, and due to the invariance of the effective potential V_e under the transformation $\theta \longrightarrow \pi - \theta$, the phase flow in this figure has been represented in the "extended" plane ($0 \geq \theta \leq 2\pi,\ P_\theta$). In region L_1, the phase flow is made of three different regions of motion. One region of rotational orbits R above the homoclinic orbit (separatrix) passing through E_2 and, below this separatrix, two nested regions of vibrational orbits V_3 and V_1 around the stable equilibrium E_3 and above the separatrix passing through E_1, respectively. The V_3 family corresponds to molecular oscillations around E_3, while V_1 levels correspond to oscillations around the positive z-axis. Note that the presence of the separatrix passing through E_1 prevents strong molecular orientation along the static electric field. On the other hand, the presence of the levels V_3 indicates that the circularly polarized laser field ($w_2 > 0$) is able to create dynamic regions where the molecule vibrates away from the z-axis. In fact, when $w_2 \gg w_1$ (i.e., $\theta_3 \to \pi/2$) levels V_3 oscillate around the polarization xy-plane of the laser field. The family R corresponds to dynamic situations where the molecule describes complete rotations.

As a consequence of the first pitchfork bifurcation, in region L_2 the phase space structure changes because the vibrational levels V_3 have disappeared. Now, V_1 levels correspond to genuine oscillations around the (stable) equilibrium E_1, which allows strong molecular orientation along the positive z-axis. This dynamic situation is analogous to the well-known pendular states [4] appearing for a static electric field ($w_2 = 0$).

After the second pitchfork bifurcation, in region L_3 appears a new kind of vibrational levels around E_2. We name these vibrational orbits as V_2. In this region the laser field is linearly polarized ($w_2 < 0$), and the V_2 levels correspond to molecular oscillations around the negative z-axis. That is to say, the molecule is mainly oriented in the opposite sense of the polarization axis of the fields.

Finally, we remark the presence of a heteroclinic-connection bifurcation when $w_1 = 0$ and $w_2 > 0$. Note that when w_1 approaches zero, the homoclinic loops that respectively are attached to E_1 and E_2 tends to merge, in such a way that, when $w_1 = 0$ the unstable equilibrium points E_1 and E_2 have the same energy (see Fig. 1) and they are connected by the same heteroclinic orbit.

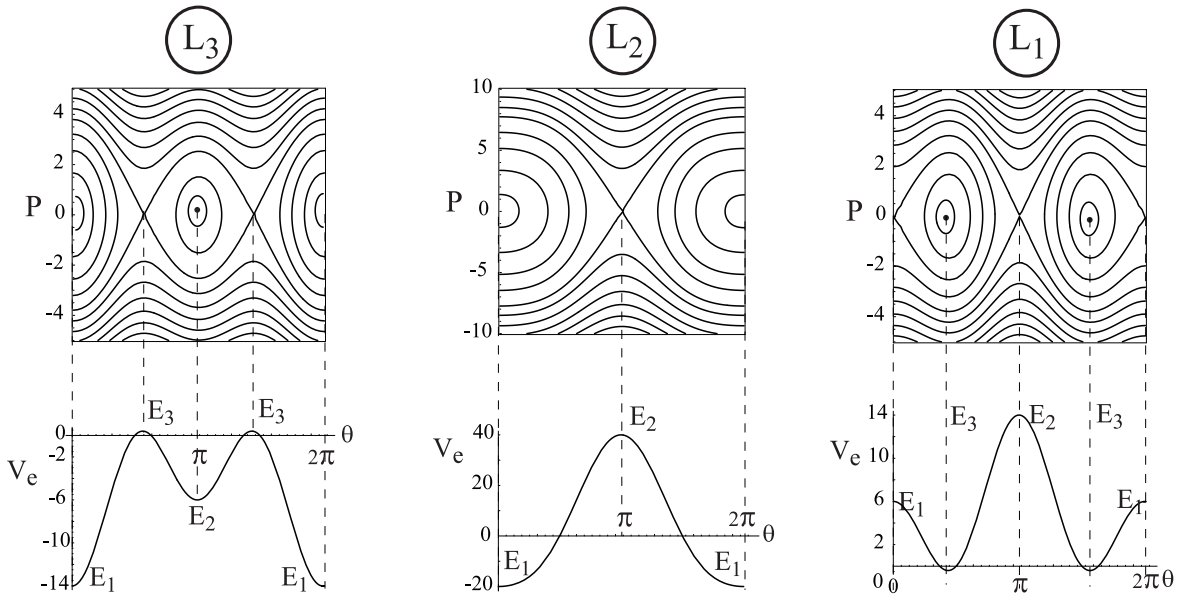

Fig. 2. Phase flow evolution and effective potential V_e for $m = 0$ as a function of the parameters (w_1, w_2). From left to right: $w_1 = 4$ and $w_2 = -10$; $w_1 = 30$ and $w_2 = 10$; $w_1 = 4$ and $w_2 = 10$.

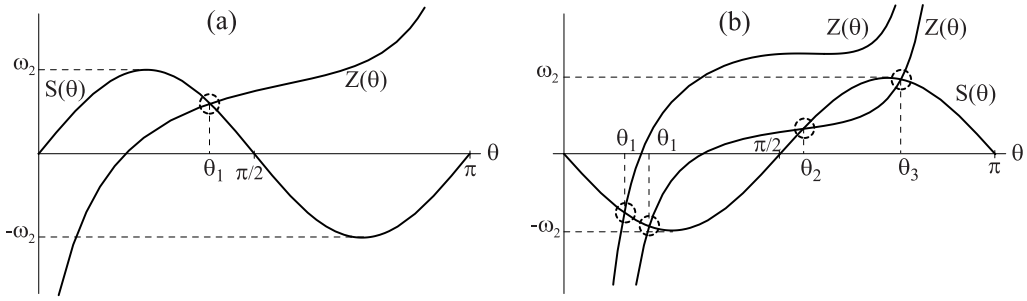

Fig. 3. Sketch of the polynomials $\mathcal{Z}(\theta)$ and $\mathcal{S}(\theta)$. The roots of $\mathcal{P}(\theta) = \mathcal{Z}(\theta) - \mathcal{S}(\theta)$ appear encircled. (a) Case $w_2 \geq 0$; (b) case $w_2 < 0$.

3.2 Case m ≠ 0

When $m \neq 0$ the effective potential V_e tends to infinity at $\theta = 0$ and $\theta = \pi$ and the critical points, when they exist, are located in the interior of the interval $(0, \pi)$.

3.2.1 Case $w_1 = 0$

In the case $w_1 = 0$, equation (7) reads as

$$-\frac{2\cos\theta}{\sin^3\theta}(m^2 + w_2 \sin^4\theta) = 0, \qquad (10)$$

and the problem presents three equilibrium points θ_1, θ_2 and θ_3, namely

$$\theta_1 = \pi/2, \quad \theta_2 = \arcsin[(-m^2/w_2)^{1/4}],$$

$$\theta_3 = \pi - \arcsin[(-m^2/w_2)^{1/4}],$$

and the corresponding characteristic eigenvalues are:

$$\lambda_1 = \sqrt{-2\ (m^2 + w_2)},$$

$$\lambda_{2,3} = 2\sqrt{-2w_2\left(\sqrt{-m^2/w_2} - 1\right)}.$$

When $w_2 < 0$ and $-m^2/w_2 \leq 1$, the three equilibria exist, being θ_1 unstable and $\theta_{2,3}$ stable. Otherwise, only θ_1 exists, being stable. Hence, for $w_1 = 0$, at $-m^2/w_2 = 1$ a pitchfork bifurcation occurs [11].

3.2.2 Case $w_1 \neq 0$

Now, we express equation (7) as: $\mathcal{P}(\theta) = \mathcal{Z}(\theta) - \mathcal{S}(\theta) = 0$,

$$\mathcal{Z}(\theta) = -\frac{2m^2\ \cos\theta}{\sin^3\theta} + w_1 \sin\theta, \qquad \mathcal{S}(\theta) = w_2\ \sin 2\theta.$$

When $w_2 \geq 0$, the direct application of the Bolzano theorem as well as the increasing and decreasing behavior of $\mathcal{Z}$ and $\mathcal{S}$ (see Fig. 3a) ensure that these functions intersect always one and only once in the interval $(0, \pi/2)$. Thence, the effective potential V_e presents a unique critical point θ_1 in that interval. Moreover, because V_e tends to infinity at $\theta = 0$ and $\theta = \pi$, θ_1 is a minimum, i.e. it corresponds to an stable equilibrium $E_1 = (\theta_1, 0)$. When $w_2 < 0$, the same study ensures that the number of crossings between $\mathcal{Z}$ and $\mathcal{S}$ is either one or three (see Fig. 3b) and the system has one or three equilibria depending on the values of the parameters. In this case, note that one of

the roots takes always place in the interval $(0, \pi/2]$, while the other two, when they exist, are located in the interval $(\pi/2, \pi)$. Let $\theta_1 < \theta_2 < \theta_3$ be such roots. Due that $V_e(\theta = 0) \to \infty$ and $V_e(\theta = \pi) \to \infty$, θ_1 and θ_3 are minima (stable equilibria E_1 and E_3) while θ_2 is a maximum (unstable equilibrium E_2).

From equation (7) we get the following fifth-degree polynomial equation

$$\mathcal{F}(x) = 2w_2x^5 - w_1x^4 - 4w_2x^3 + 2w_1x^2 + (2m^2 + 2w_2)x - w_1 = 0, \qquad x = \cos\theta, \quad (11)$$

and the equilibrium points of the problem are its real roots in the interval $(-1, 1)$. However, the polynomial $\mathcal{F}$ being of degree 5 in x, there are no general formulae giving its roots in exact terms. For this reason, we focus on when the number of roots is one or three. Because we have shown that there is always at least one root in the interval $(0, \pi)$, we take advantage of the resultant of a polynomial [16] to compute the boundary between one or three roots, which corresponds to the appearance of a double root $\theta_2 = \theta_3$ in the interval $(\pi/2, \pi)$. In this way the resultant is given by

$$\begin{aligned} Res\left(\mathcal{F}, \frac{d\mathcal{F}}{dx}\right) = 32\ m^4\ w_2(&4096\ w_2^6 + 12288\ m^2\ w_2^5 \\ &+ (12288\ m^4 - 3072\ w_1^2)\ w_2^4 \\ &+ (4096m^6 + 11136m^2w_1^2)w_2^3 \\ &+ (384m^4w_1^2 + 768w_1^4)w_2^2 - 96m^2w_1^4w_2 \\ &- 64w_1^6 - 27m^4w_1^4) = 0. \end{aligned} \quad (12)$$

Excluding the cases $m = 0$ and $w_1 = 0$, polynomial $\mathcal{F}$ has a double root when the last factor of (12) vanishes. That is to say, when

$$\begin{aligned} \Gamma = &4096\ w_2^6 + 12288\ m^2\ w_2^5 \\ &+ (12288\ m^4 - 3072\ w_1^2)\ w_2^4 \\ &+ (4096m^6 + 11136m^2w_1^2)w_2^3 \\ &+ (384m^4w_1^2 + 768w_1^4)w_2^2 - 96m^2w_1^4w_2 \\ &- 64w_1^6 - 27m^4w_1^4 = 0. \end{aligned} \quad (13)$$

From this discussion, once m is fixed, the parametric plane $(w_2,\ w_1)$ divides in two different regions where the number of roots (equilibria) is either one or three (see Fig. 4). These regions are kept apart by the curve defined by $\Gamma = 0$ as it is depicted in Figure 4. This curve corresponds to a parametric bifurcation of saddle-center type. At this point, it is worth notice that, when $m = 0$, Γ is given by

$$\Gamma = -64(w_1 - 2\ w_2)^3(w_1 + 2\ w_2)^3 = 0, \quad (14)$$

which describes the two pitchfork bifurcation lines $w_1 = \pm 2\ w_2$ for the case $m = 0$. Moreover, when $w_1 = 0$, we have that

$$\Gamma(w_1 = 0) = 4096\ w_2^3(m^2 + w_2)^3 = 0,$$

which gives the pitchfork bifurcation taking place for $w_1 = 0$ at $m^2 = -w_2$.

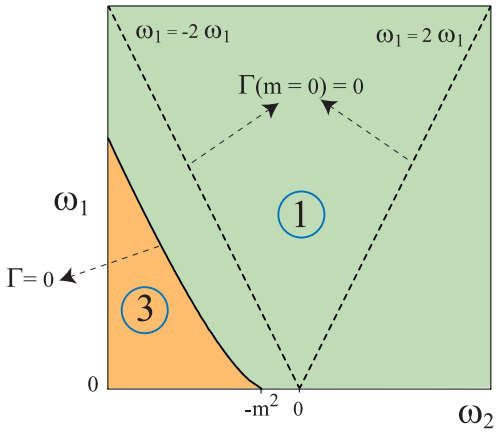

Fig. 4. Plane of parameters (w_2, w_1) for a given m. The number of equilibria in each region delimited by the curve $\Gamma(m \neq 0) = 0$ appears encircle. The dashed lines are the bifurcations lines $w_1 = \pm 2w_2$ for $m = 0$ ($\Gamma(m = 0) = 0$).

In order to corroborate analytically the stability behavior of the equilibrium points $(\theta_1, \theta_2, \theta_3)$ we are compelled to study the sign of the corresponding characteristic eigenvalues. This study reduces to study the sign of the polynomial

$$\xi(x) = 4w_2x^6 - w_1x^5 - 10w_2x^4 + 2w_1x^3 + 4(2w_2 - m^2)x^2 - w_1x - 2m^2 - 2w_2, \qquad x = \cos\theta, \quad (15)$$

evaluated at the critical points $(\theta_1, \theta_2, \theta_3)$ in the interval $-1 < x < 1$. However, instead of checking the sign of (15) (which is not a simple task), we show that equilibria conserve their stability properties. Indeed, let us calculate the resultant of the polynomials $\xi(x)$ and $\mathcal{F}(x)$, which reads as

$$\begin{aligned} Res(\xi, \mathcal{F}) = -128\ m^8\ w_2\Big(&4096\ w_2^6 + 12288\ m^2\ w_2^5 \\ &+ \left(12288\ m^4 - 3072\ w_1^2\right)\ w_2^4 \\ &+ \left(4096m^6 + 11136m^2w_1^2\right)\ w_2^3 \\ &+ \left(384m^4w_1^2 + 768w_1^4\right)\ w_2^2 \\ &- 96m^2w_1^4w_2 - 64w_1^6 - 27m^4w_1^4\Big). \end{aligned} \quad (16)$$

Note, that excluding the cases $m = 0$ and $w_2 = 0$, equation (16) vanishes with $Res(\mathcal{F}, d\mathcal{F}/dx)$. Then, the equilibria $(\theta_1, \theta_2, \theta_3)$ conserve their stability while they exist.

In accordance with the previous study, we find two different phase portrait. When there are three equilibria (see left panel in Fig. 5), the phase flow is made of three different regions of motion: one region of rotational orbits R above the separatrix passing through E_2 and two zones of vibrational orbits V_1 and V_3 around the stable equilibria E_1 and E_3 respectively. In this region, despite the strength of the static electric field, the linearly polarized laser dominates the dynamics because the presence of the families V_1 and V_3 indicates that the molecular axis is oriented along either the positive or the negative z-axis. As we approach $\Gamma = 0$, the deep of the potential well on the right

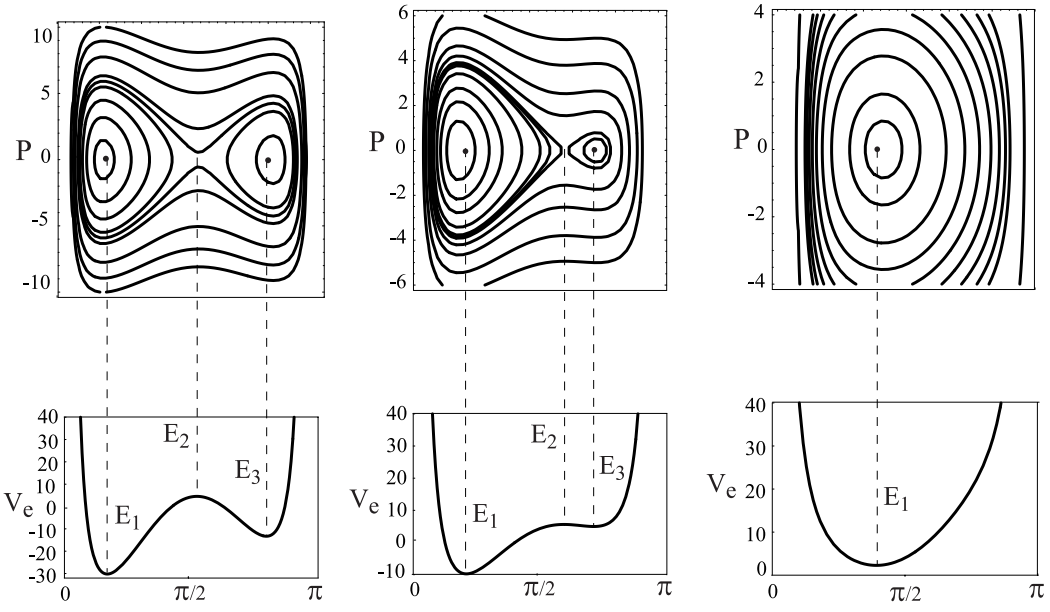

Fig. 5. Phase flow evolution and effective potential for $m = 2$ and $w_1 = 10$ as a function of the parameter w_2. From left to right: $w_2 = -50$; $w_2 = -20$; $w_2 = 10$.

decreases while the deep of the left-hand potential well increases. Therefore, the equilibria E_2 and E_3 move one to each other (see central panel in Fig. 5) and the vibrational levels V_3 tend to disappear. When the bifurcation takes place, only the potential well passing through the minimum E_1 exists and the phase flow is made of oscillations around the equilibrium point E_1 (see Fig. 5). In this pendular-like situation the static electric field dominates the dynamics.

Note that the saddle-node bifurcation not only causes the extinction of the vibrational levels V_3 but also the distinction between rotational and vibrational levels. In this pendular regime, the molecule describes oscillations which amplitudes just depend on the energy. The smaller the energy is, the more localized the molecular oscillation is around the equilibrium E_1. In other words, as the energy increases, it takes place a smooth evolution from orbits strongly oriented along the positive z-axis to non oriented orbits.

4 Quantum mechanical consequences of the saddle-node bifurcation

The objective of this Section is to study how the bifurcations taking place in this problem affect the orientation of the quantum states. In particular, we focus on the saddle-node bifurcation.

To calculate the states of the quantum mechanical Hamiltonian $\widehat{H}$ associated to (4), we solve the usual secular equations that arise from the expansion of the wave function Ψ in terms of the spherical harmonics $Y_{j,m}(\theta, \phi)$, the eigenfunctions of the free-rotor. Since m is a good quantum number, its value remains the same for a given m expansion, and the so-called pendular states $\Psi_{J,m}$,

$$\Psi_{J,m}(\theta, \phi) = (J, m) = \sum_{j=m} c_{J;j,m} Y_{j,m}(\theta, \phi), \qquad (17)$$

are labeled with m and with the symbol J. This symbol corresponds to the value of j of the free-rotor state that for $w_1 \to 0$ and $w_2 \to 0$ the hybrid state (J, m) correlates. If only the laser field is present ($w_1 = 0$), the eigenfunctions resulting from (17) have definite parity $(-1)^j$, while when the static field is present ($w_1 \neq 0$) the eigenfunctions have not definite parity.

Now, following a similar procedure as Friedrich and Herschbach in [7], we fix the values $m = 2$ and $w_2 = -50$ and we track the evolution of the two lowest states $(2, 2)$ and $(3, 2)$. Because $w_2 < -m^2$, when the static field is turned off, the effective potential (6) has two symmetric potential wells, and as we can observe in Figure 6a, $(2, 2)$ and $(3, 2)$ form a nearly degenerate doublet of states aligned along the z-axis. We note that neither fully alignment nor fully orientation are possible due to the centrifugal term in the effective potential (6).

As soon as the static electric field is turned on, the doublet splits and opposite orientations are obtained (see Fig. 6b): positive for $(2, 2)$ and negative for $(3, 2)$. Now, the $(2, 2)$ and $(3, 2)$ states are located, respectively, at the left-hand and at the right-hand potential wells. From a classical point of view, they correspond to a V_1 level and to a V_3 level. Because the orientation of the $(2, 2)$ state remains almost constant as w_1 increases, we pay our attention to the evolution of the $(3, 2)$ state. Between $w_1 = 13$ and $w_1 = 15$, the $(3, 2)$ wave function undergoes a fast positive reorientation (see Figs. 6c and 6d). In this new situation, the state is also laying in the left-hand side potential well and it corresponds to a classical V_1 level. When $w_1 > 20$ the state $(3, 2)$ is almost completely oriented towards the positive z-axis (see Figs. 6e and 6f).

We can visualize the above orientation process from a different and deeper point of view. The expectation value $\widehat{c}_{Jm} = \langle \cos\theta \rangle_{Jm}$ characterizes the extent of the orientation of a given (J, m) state. We use this quantity to investigate the evolution of the orientation of the four

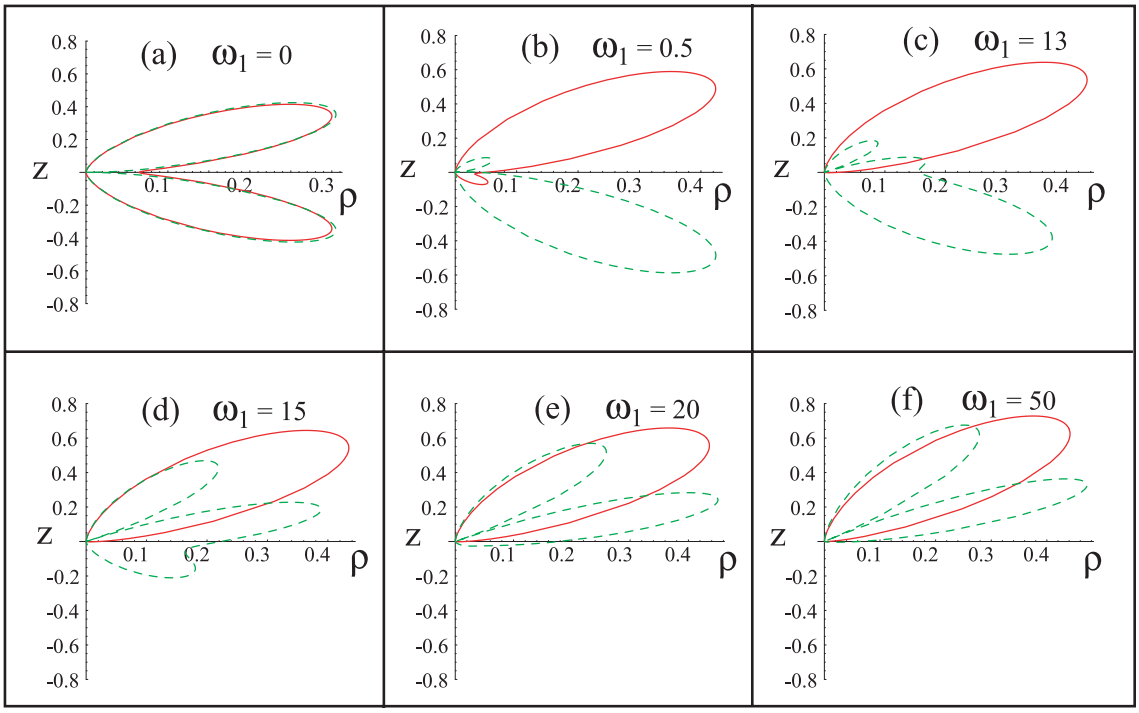

Fig. 6. Evolution of the states $|22\rangle$ (solid line) and $|32\rangle$ (dashed line) for $w_2 = -50$ as a function of w_1.

lowest $(2,2)$, $(3,2)$, $(4,2)$ and $(5,2)$ states. The result of this study is displayed in Figure 7. Roughly speaking, when $w_1 > 50$, we find that Figure 7a for $w_2 = 0$ and Figure 7b for $w_2 = -50$ show qualitatively the same $\widehat{c}_{Jm}$ evolution: a monotonic increasing of the orientation of the states as w_1 grows. In this pendular-like region, the static electric field dominates the dynamics. Note that, for $m = 2$ and $w_2 = -50$, the equation (13) gives the saddle-node bifurcation value $w_{1c} \approx 49.428706$. For $w_1 > w_{1c}$, the effective potential (6) shows only one potential well. The value w_{1c} agrees very well with the value $w_1 \approx 50$ from which, in Figure 7b, the pendular regime prevails.

However, when $w_1 < 50$, a more complex behavior is observed because (6) has two potential wells. For $w_1 < 13$, the lowest $(2,2)$, $(3,2)$ and $(4,2)$ states are strongly oriented along the positive or the negative z-axis. In this interval, the laser field dominates the dynamics because the two potential wells of (6) are deep enough to bind the three states. However, this situation will change because, as w_1 increases, the deep of the right-hand well decreases and the competition between the fields is served. In the interval $13 < w_1 < 15$, $\widehat{c}_{32}$ shows an abrupt change from negative to positive values while in the same interval, $\widehat{c}_{42}$ changes from positive to negative. These fast reorientations indicate that the states "jumped" from one potential well to another: the $(3,2)$ state from the well on the right to the well on the left, and the $(4,2)$ state from the well on the left to the well on the right. Note that the change of $\widehat{c}_{32}$ describes the fast reorientation process of the $(3,2)$ state displayed in Figure 6. When $w_1 > 15$, $\widehat{c}_{32}$ increases monotonically. In the interval $20 < w_1 < 40$, $\widehat{c}_{42}$ becomes again positive because the $(4,2)$ state moves to the left-hand well because the right-hand one is not able to bind

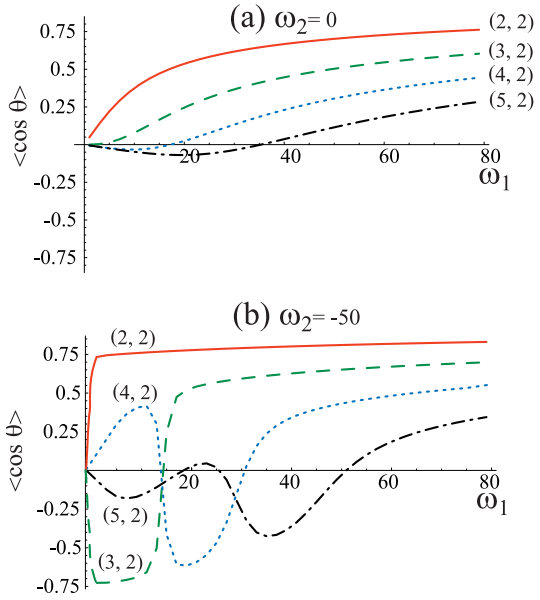

Fig. 7. Evolution of the orientation $\langle \cos\theta \rangle_{Jm}$ for the states $(2,2)$, $(3,2)$, $(4,2)$ and $(5,2)$ for (a) $w_2 = 0$, and (b) $w_2 = -50$ as a function of w_1.

this state. For $w_1 > 40$, the $(4,2)$ state undergoes a positive and definitive reorientation. The orientation $\widehat{c}_{52}$ of the $(5,2)$ state describes smooth oscillations around zero until, by $w_1 = 50$, suffers a outstanding and final positive reorientation.

From the above study, we deduce that the saddle-node bifurcation acts like a rough quantum frontier from which the pendular regime prevails. It is important to

understand where is this frontier because this field configuration has been widely used not only in theoretical studies but also in experiments to control and manipulate the orientation of molecules (see [6,7] and references therein).

5 Conclusions

As we noted in the Introduction, Joyeux et al. [10] and Arango et al. [11,13] detected pitchfork and saddle-node bifurcations in the phase flow of the system at hand. While the appearance of the pitchfork bifurcations was established on analytical grounds, the saddle-node bifurcation was detected by numerical investigations. In this paper, we proved analytically the nature of this saddle-node bifurcation as well as the we found the curve in the parameter space where the bifurcation takes place. This bifurcation curve allows us to give a complete description of the classical dynamics of the molecule as a function of the parameters. Finally, we have studied the impact of the classical saddle-node bifurcation on the orientation of the quantum states.

This research has been supported by the Spanish Ministry of Science and Technology (DGI Project No. MTM2005-08595).

References

1. P. Langevin, J. Phys. **4**, 678 (1905)
2. P. Debye, *Polar molecules* (Chemical Catalogue, reprinted by Dover, New York, 1929)
3. H. Stapelfeldt, T. Seideman, Rev. Mod. Phys. **75**, 543 (2003)
4. J.M. Rost, J.C. Griffin, B. Friedrich, D.R. Herschbach, Phys. Rev. Lett. **68**, 1299 (1992)
5. B. Friedrich, D.R. Herschbach, J. Phys. Chem. **99**, 15686 (1995)
6. B. Friedrich, D.R. Herschbach, J. Chem. Phys. **111**, 6157 (1999)
7. B. Friedrich, D.R. Herschbach, J. Phys. Chem. A **103**, 10280 (1999)
8. L. Cai, J. Marango, B. Friedrich, Phys. Rev. Lett. **86**, 775 (2001)
9. H. Sakai, S. Minemoto, H. Nanjo, H. Tanji, T. Suzuki, Phys. Rev. Lett. **90**, 083001 (2003); S. Minemoto, H. Nanjo, H. Tanji, T. Suzuki, H. Sakai, J. Chem. Phys. **118**, 4052 (2003)
10. M. Joyeux, S.C. Farantos, R. Schinke, J. Phys. Chem. A **106**, 5407 (2002)
11. C.A. Arango, W.W. Kennerly, G. Ezra, J. Chem. Phys. **122**, 184303 (2005)
12. R. Cushman, L. Bates, *Global aspects of classical integrable systems* (Birkhauser Verlag, Besel, Switzerland, 1997); D.A. Sadovskií, B.I. Zhilinskií, Phys. Lett. A **256**, 235 (1999); I.N. Kozin, R.M. Roberts, J. Chem. Phys. **118**, 10523 (2003); K. Efstathiou, M. Joyeux, D.A. Sadovskií, Phys. Rev. A **69**, 032504 (2004)
13. C.A. Arango, W.W. Kennerly, G. Ezra, Chem. Phys. Lett. **392**, 486 (2004)
14. A. Elipe, A. Abad, A. Deprit, Int. J. Non-Linear Mech. **36**, 693 (2001)
15. As it is noted by Arango et al. [13], if we consider $w_2 \neq 0$ the quotient $\mathcal{A} = w_1/2w_2$ is the effective parameter that controls the dynamics. We prefer to use w_1 and w_2 separately in order to consider a continuous variation of w_2.
16. D. Cox, J. Little, D. O'Shea, *Ideals, Varieties and Algorithms: An Introduction to Computational Algebraic Geometry and Commutative Algebra* (Springer–Verlag, Berlin and New York, 1992).